



Synthesis of locust bean gum/titanium dioxide hydrogel nanocomposites for efficient removal of methylene blue from aqueous solution

Boitumelo Rejoice Motshabi¹ · Edwin Makhado¹ · Nompumelelo Malatji¹ · Kwena Desmond Modibane¹ · Mpitloane Joseph Hato² · Orebotse Joseph Botlhoko² · Mahmoud H. Abu Elella³

Accepted: 18 February 2024
© The Author(s) 2024

Abstract

In this study, we are interested in preparing novel hydrogel and hydrogel nanocomposite-based adsorbents for removing methylene blue (MB) dye based on grafted locust bean gum (LBG). LBG hydrogel and hydrogel nanocomposite were synthesized using a radical polymerization technique in the absence and presence of TiO₂ with LBG-cl-(acrylic acid (AA)-co-acrylamide (AAm)). Various analytical instruments Fourier transform infrared (FTIR), X-Ray diffraction (XRD), Scanning electron microscopy (SEM), and High-resolution transmission electron microscopy (HRTEM) were used to elucidate the chemical structure and surface morphology of the prepared samples. Using a batch adsorption experiment, the Langmuir isotherm model showed that LBG-cl-p(AA-co-AAm) hydrogel had a maximum adsorption capacity of 1540.9 mg/g and LBG-cl-(AA-co-AAm)/TiO₂ hydrogel nanocomposites had a maximum adsorption capacity of 1273.4 mg/g at neutral pH. The thermodynamic data demonstrated that MB dye was removed via spontaneous adsorption. Furthermore, the regeneration study showed good recyclability for the obtained hydrogel nanocomposites through six consecutive reusable cycles. Therefore, the hydrogel nanocomposites are an effective adsorbent for the removal of MB dye from aqueous solutions.

Keywords Locust bean gum · Wastewater · Methylene blue · Titanium dioxide · Hydrogel nanocomposite

Introduction

Water is one of the most crucial needs for human life and the ecosystem as well. Over the past decades, notably, water pollution has resulted in the discharge of toxic effluents onto water surfaces because of fast-paced industrialization and a rising population. Thereby, it endangers the health of

people and the ecosystem as well. Water pollution occurs as a result of the release of toxic chemical pollutants like synthetic organic dyes [31]. Synthetic organic dyes are utilized in many industrial areas, for example, textiles, which cause a large amount of contamination in our environment. Cationic dyes are the primary source of contaminated water. Several published reports mentioned that these dyes are non-biodegradable materials and do not degrade easily via conventional treatment techniques. As a result, they accumulate in living cells and cause fatal diseases. Widespread fabrics are dyed with cationic-charged substances, including methylene blue (MB), malachite green (MG), crystal violet (CV), methyl violet (MV), and others. Several adverse effects are associated with MB, which can cause blindness, skin irritation, respiratory difficulties, migraines, and dizziness [17, 41, 42].

To solve this environmental problem, various conventional techniques can be applied for the purification of dye-based contaminated water, including electrochemical [21], catalytic degradation [51], membrane separation [3], photo-degradation [16], and coagulation-flocculation [15].

✉ Edwin Makhado
edwin.makhado@ul.ac.za; edwinmakhado@yahoo.com

✉ Mahmoud H. Abu Elella
mhussien@cu.edu.eg

¹ Department of Chemistry, School of Physical and Mineral Sciences, University of Limpopo, Sovenga, Polokwane 0727, South Africa

² Centre for Nanostructures and Advanced Materials, DSI-CSIR Nanotechnology Innovation Centre, Council for Scientific and Industrial Research, Pretoria 0001, South Africa

³ Chemistry Department, Faculty of Science, Cairo University, Giza 12613, Egypt

Traditional purification strategies, on the other hand, have outstanding disadvantages: low dye separation, high energy and time consumption, high-cost techniques, and limited function. Recently, the adsorption approach has drawn intensive attention for heavy metals, pharmaceuticals, and dye-based wastewater [54] purification thanks to its advantages, such as high-selectivity and low-cost technique, as well as its straightforward operation [2, 46]. Recently, polysaccharide-based adsorbents have played a crucial role in wastewater treatment applications thanks to their remarkable features, such as being highly stable, inexpensive, nontoxic, biodegradable, widely available, and environmentally friendly [25, 25, 26, 26, 29, 29, 36, 46]. Various polysaccharide formulation-based adsorbents can be widely applied for the removal of toxic synthetic dyes from contaminated water. Included in the aforementioned studies are hydrogels [1]; [35, 50] and formulation of hydrogel nanocomposites [9, 34, 37].

Hydrogels are three-dimensional polymeric structures. They can absorb biological fluids and water and resemble biological tissues without dissolving their compositions; therefore, they are called smart materials [4, 25, 26, 29, 30]. Hydrogels are intensively used for removing various dyes due to their unique properties like fast kinetics, recyclability, good adsorption performance, and low cost [7, 57]. Several efforts have been made to develop hydrogels from natural polymers like polysaccharides to reduce the total cost of the adsorption materials [2, 7]. Hydrogel-based polysaccharides like locust bean gum (LBG) have received potential interest in the last few years [5, 43]. For example, in 2020, Pandey et al. mentioned the synthesis of LBG hydrogel-based adsorbents for capturing brilliant green (BG) dye with a Q_{max} of 142.85 mg/g, fitted with the Langmuir model [40]. In a separate study, most recently, the LBG hydrogel nanocomposites were prepared via in-situ iron mineralization within hydrogel chains for capturing methyl violet and MB dyes. They reported that the prepared LBG hydrogel nanocomposites had outstanding adsorption efficiency as well as excellent regeneration ability [41, 42]. Recently, various scientific groups worldwide have shown great interest in designing hydrogel nanocomposites by incorporating different inorganic nanoparticles as nanofillers within polymeric hydrogel matrixes [18, 22]. Hydrogel nanocomposites are widely employed as adsorbents for water purification by adsorbing trace levels of metal ions, organic dyes, and other contaminants. Owing to their high adsorption capacity, swelling ability, recyclability, and good thermomechanical stability, which intensifies their usage for environmental remediation. In this direction, several researchers have integrated nanoparticles (e.g., Fe_3O_4 , ZnO, and TiO_2) into the polymeric hydrogel matrix to develop adsorbents with superior properties [27, 32, 45].

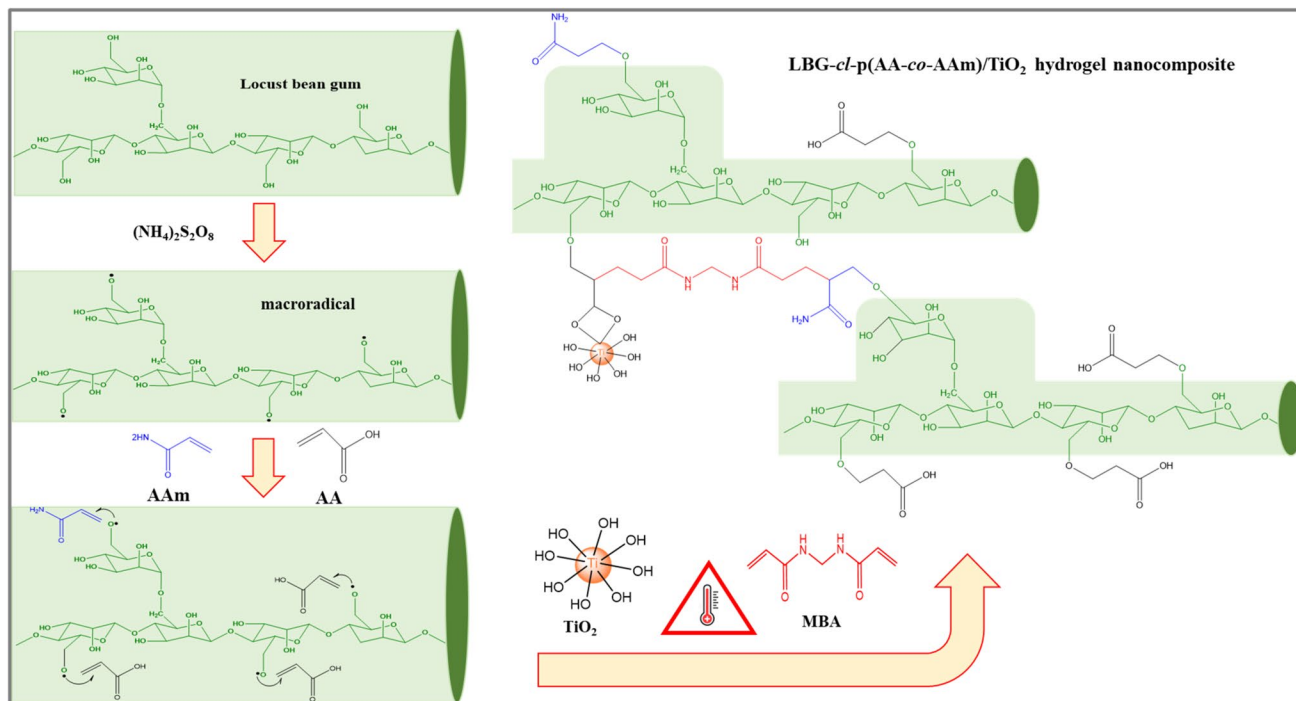
Among nanostructured metal oxides, TiO_2 nanoparticles have attracted potential interest owing to their remarkable properties, including their accessibility, high specific surface area, tunable interlayer spacing, versatility, surface hydrophilicity, and photocatalytic activity [59, 38]. Nano-sized TiO_2 nanoparticles can interact intact with functional groups of hydrogel networks and increase the centre of negative charge within the hydrogel network to improve their binding to positively charged dye molecules [23]. Moreover, many published studies have reported that the incorporation of TiO_2 nanoparticles can enhance the physiochemical properties of hydrogels [55, 60]. Our prior study showed this phenomenon, which was well demonstrated by constructing hydrogel nanocomposites containing TiO_2 nanoparticles and strengthening their mechanical elasticity; however, their swelling ability in water decreased [23]. According to the literature, it is expected that the addition of TiO_2 nanoparticles within hydrogel chains will improve their adsorption performance, mechanical and thermal stabilities [23, 55].

With radical polymerization of LBG, acrylamide, and acrylic acid monomers and N,N'-methylenebisacrylamide as a crosslinker, without and with nano-sized TiO_2 , a LBG hydrogel and a hydrogel nanocomposites-based MB adsorbent were successfully synthesized. The analysis of the prepared samples was conducted using several techniques, including FTIR, XRD, SEM, and TEM, in order to examine both their chemical composition and surface morphology. The study examined the impact of several factors, such as solution pH, adsorbent dosage, equilibrium concentration, temperature, and contact time, on the sorption capacity of the LBG-cl-p(AA-co-AAm) hydrogel and its nanocomposites for MB dye. Additionally, investigations were conducted to investigate the adsorption kinetics, isotherms, and thermodynamics. A desorption-adsorption study was also performed to determine the recyclability of LBG-cl-p(AA-co-AAm) hydrogel and its nanocomposites-based adsorbents.

Experimental Section

Materials

The locust bean gum (LBG) from *Ceratonia siliqua* seeds, acrylic acid (AA, 99%), acrylamide (AAm, 99%), ammonium persulfate ($\geq 98.0\%$; 248614), methylenebisacrylamide (MBA, 99%), MB dye, titanium isopropoxide (97%), nitric acid (65%), and propan-2-ol were obtained from Sigma-Aldrich. Acetone, sodium hydroxide (NaOH), and hydrochloric acid (HCl, 37%) were collected from Merck. Deionized water was used in all studies. Standard methylene



Scheme 1 Schematic illustration of the synthesis of LBG-cl-(AA-co-AAm)/TiO₂ HNCs

blue (MB) dye solution was prepared by dissolving 1g of MB dye in 1L of deionized water, followed by subsequent dilution.

Preparation of TiO₂ Nanoparticles (NPs)

TiO₂ was synthesised according to our previous reported work in the literature [23] via a conventional sol-gel technique. Briefly, initially, titanium isopropoxide (10 ml) was dissolved with propan-2-ol (30 mL). Next, a turbid solution was obtained after 20 min of magnetic stirring, and deionized water (10 mL) was added. After that, nitric acid was slowly added to decrease the pH of the solution, and the mixture was left for 15 min. After 15 min, a yellow precipitate was formed by drying the mixture at 80 °C. The powder of TiO₂ NPs was obtained by grinding the material to a fine consistency and then calcining it at 600 °C.

Preparation of LBG-cl-p(AA-co-AAm) Hydrogel

LBG-cl-p(AA-co-AAm) hydrogel was prepared according to the following method. In the beginning, 100 mg of LBG powder was dissolved in deionized water (10 mL). Next, 20 × 10⁻³ M of initiator (APS) was added to the LBG solution. Subsequently, the optimum amount of AA (10 × 10⁻⁴ M) was added to the above solution. While 60 × 10⁻³ M of AAm was first dissolved firstly using deionized water (3 mL) in a separate container and then

added to the aforementioned reaction mixture, that was followed by 0.1 × 10⁻¹ M of MBA addition. The reaction was kept at 30 mL under continuous magnetic stirring at 70 °C for 2 h. After 2 h, the resulting solution cooled at room temperature (-25 °C). Then, the final hydrogel product was cut into smaller pieces, and then immersed in acetone for 120 min to withdraw all homopolymers. Finally, the purified modified LBG oven-dried at 60 °C, and pulverized into a fine powder for further investigation.

Preparation of LBG-cl-p(AA-co-AAm)/TiO₂ Hydrogel Nanocomposites (HNCs)

In a typical process as depicted in Scheme 1, LBG hydrogel nanocomposites was synthesized with the same procedure that was described above with the addition of 0.1 g of TiO₂ nanoparticles to the beaker holding the LBG, APS, AA, AAM, and MBA. For 20 min, the solution was agitated at 25 °C to provide a homogeneous mixture. Subsequently, the solution was left for 2 h at 70 °C. After 2 h, the resulting solution cooled within 30 min at room temperature (-25 °C). After that, the product cut into tiny pieces, and then immersed in acetone for 120 min to separate all homopolymers. Finally, the prepared adsorbent was oven-dried at 60 °C and pulverized into a fine powder using a mill ball for further investigation.

Characterization Methods

Scanning electron microscopy (SEM) was used to look into the morphology of sample surface ((FESEM) SEM, JSM7500F, JOEL, Japan). The SEM was coupled with EDS (energy dispersive X-ray spectrometer). Fourier transform infrared (FTIR) spectra with a resolution of 4 cm^{-1} were acquired in the $400\text{--}4000\text{ cm}^{-1}$ wavenumber range. A PAnalytical Xpert PRO diffractometer (PAnalytical) was applied to acquire XRD. Evaluation of thermal stability performed with thermal gravimetric analysis ((TGA), Perkin-Elmer STA 6000) between 30 and $900\text{ }^{\circ}\text{C}$ under in a N_2 using 20 mL/min of flow rate. High-resolution transmission electron microscopy (HRTEM) (JEOL JEM-2100, Tokyo, Japan) was applied to investigate internal morphology of samples with integrated SAED (Selected Area Electron Diffraction). The mechanical stability of the materials was studied dynamically at temperature of $30\text{ }^{\circ}\text{C}$ and a frequency band that ranges from 0.01 to 100 Hz , with a 0.05% of strain amplitude and $5\text{ }^{\circ}\text{C/min}$ of ramp rate using the dynamic mechanical analysis ((DMA), 8000 Perkin-Elmer, USA). The remained concentration of MB dye was measured with LAMBDA 365 UV-Vis Spectrophotometer.

Swelling Ability

The degree of swelling ability for both LBG-cl-p(AA-co-AAm) hydrogel and LBG-cl-(AA-co-AAm)/ TiO_2 HNCs was studied using deionized water as follows: 0.1 g of modified LBG samples were typically soaked in 80 mL of various pH solutions ranging from pH 1.0 to pH 9.0. The pH was adjusted with HCl (0.1 M) and NaOH (0.1 M). The effect of inorganic salts (NaCl , CaCl_2 , and FeCl_3) on the swelling behavior of the adsorbent was examined. After letting the adsorbent soak in the deionized water for 24 h , we weighed it again after wiping it off with filter paper in order to estimate its equilibrium swelling capacity. The formula for calculating the swelling capacity is as follows:

$$S(g/g) = \frac{M_s - M_d}{M_d} \quad (1)$$

where M_s is the swollen mass of modified LBG samples and M_d is the dry sorbent mass.

Adsorption Studies

The MB dye adsorption was studied with the batch method. With the optimum amount of adsorbent (0.5 g/L), 20 mL of the dye standard solutions were poured into a 100 mL PE container. Then, we put it in a water bath with a thermostatic oscillator at $25\text{ }^{\circ}\text{C}$ and set the speed to 170 rpm . Adsorption capacity was investigated at different pHs in the range of

$4.0\text{--}12.0$ and adsorbent dosages of $0.5\text{--}2.5\text{ g/L}$. In addition, the effect of time on adsorption capacities at $25\text{ }^{\circ}\text{C}$ was analyzed between 15 and 180 min throughout the adsorption process. The dosage of MB dye used in the adsorption isotherm experiments ranged from 100 to 700 mg/L . The aliquots of MB-loaded adsorbents were filtered after finishing the adsorption time directly, and the concentration was determined using a UV-Vis spectrophotometer ($\lambda_{\text{max}} = 664\text{ nm}$). The adsorption capacities (q_e) and (q_t) were calculated using the following formula:

$$q_e = \left(\frac{C_0 - C_e}{m} \right) V \quad (2)$$

$$q_t = \left(\frac{C_0 - C_e}{m} \right) V \quad (3)$$

where, C_0 and C_e are the initial and equilibrium concentrations of MB (mg/L), respectively. V is the volume of the MB solution (L), and m is the adsorbent dose (g). The variables q_e and q_t denote the equilibrium capacity of MB and the quantity of MB adsorbed per unit mass of the adsorbent (mg/g) within a particular time (t), respectively.

Analysis of Error

The non-linear adsorption isotherm models were evaluated using the root mean square error (RMSE) values. A lower RMSE value implies a better fit of the model. The literature states that when the RMSE is < 0.1 , < 0.2 , < 0.3 , and > 0.3 , the accuracy of the model is exceptional, reasonable, fair, and poor, respectively [22]. The following formula was used to determine the RMSE:

$$\text{RMSE} = \sqrt{\frac{\sum_{i=1}^N (q_{\text{exp}} - q_{\text{cal}})^2}{N}} \quad (4)$$

where q_{exp} is the experimental adsorption capacity, and q_{cal} is the estimated adsorption capacity based on the isotherm equation model, and n is the total number of data points from the experiment.

Regeneration Studies

To perform regeneration tests, MB-loaded adsorbents were immersed in 60 mL of 0.1 M HCl under continuous stirring (140 rpm) for 2 h . The recovered materials were rinsed using water and oven-dried at $40\text{ }^{\circ}\text{C}$. Subsequently, they were pulverized into powder form and reapplied in the following adsorption cycle. Six adsorption-desorption cycles were carried out.

Determination of pH of Zero Charge

pH, which includes zero total electrical charge on the surface of examined adsorbent, is called pH_{pzc}. The pH_{pzc} of fabricated modified LBG adsorbents was measured by [27]. Modified LBG adsorbents (0.1 g) was soaked in deionized water (80 mL), and then the initial solution pH adjusted to a range of 2.0–10.0 (pH_{initial}), then shaken at 170 rpm for 48 h to determine the pH_{pzc}. After 48 h, final pH (pH_{final}) was measured. The pH_{pzc} value was determined from the plotted graph between pH_{initial} and the difference between pH_{initial} and pH_{final} (Δ pH) [8].

$$\Delta pH = pH_{final} - pH_{initial} \quad (5)$$

Results and Discussion

Material Characterization

FTIR is an efficient tool for determining the structural composition of the prepared modified LBG samples compared with native LBG. The chemical structure of LBG, TiO₂ nanoparticles, LBG-cl-p(AA-co-AAm) hydrogel, and LBG-cl-p(AA-co-AAm)/TiO₂ HNCs was confirmed by FTIR analysis, as shown in Fig. 1a. TiO₂ nanoparticles revealed a variety of distinct peaks in their FTIR spectra, including an stretching vibration band at 3408 cm⁻¹ referred to O–H groups. The peak found at 1623 cm⁻¹ was attributed to the stretching vibration of Ti–OH bonds. Whereas the prominent peak observed at 521 cm⁻¹ was related to the TiO₂ bending band, which is a typical TiO₂ peak [44]. In the LBG spectrum, the stretching vibration of –OH functional groups were represented by band from 3004 to 3682 cm⁻¹, whereas the C–H functional groups CH and CH₂ was represented by peaks at 2871 and 2920 cm⁻¹. The galactose stretching and mannose rings appeared at 1648 cm⁻¹. The peaks found at

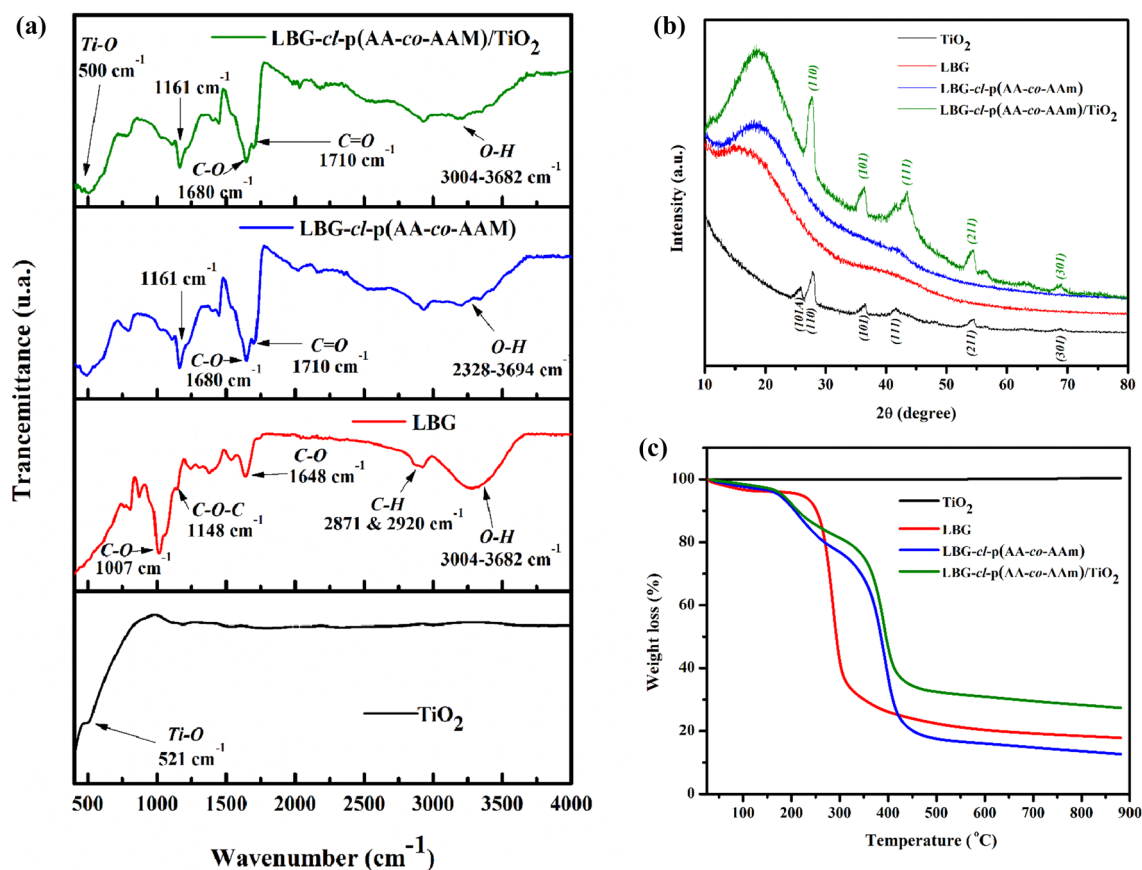


Fig. 1 **a** FTIR spectra, **b** XRD pattern and **c** TGA of TiO₂ nanoparticles, LBG, LBG-cl-p(AA-co-AAm) hydrogel and LBG-cl-p(AA-co-AAm)/TiO₂ HNCs

1441 cm^{-1} and 1380 cm^{-1} were attributed to C–H bending or CH and CH_2 deformation. The peaks detected at 950 and 1148 cm^{-1} established the linkage between C–O–C and C–O glycosidic bonds [40–42].

The LBG spectra exhibited a broad band ranging from 2328 to 3694 cm^{-1} after grafting with (AA-co-AAm). This spectral feature may be attributed to the stretching of –OH groups, which occurs due to intermolecular hydrogen bonding resulting from the chemical interaction between polyacrylic acid (pAA) and LBG. The intensity and the broadness of the galactose stretching and mannose rings appeared at 1648 cm^{-1} emanating from LBG due to the co-polymerization of AA and AAm monomers [41, 42]. Furthermore, the broad band from 1493 to 1771 cm^{-1} exhibits significant monomer structure characteristics, with the peaks induced by C=O (1710 cm^{-1}), C–O (1680 cm^{-1}), C–C (1620 cm^{-1}), and asymmetric stretching of O–C–O at 1560 cm^{-1} overlapping to form a tuned spectral range, leaving only two peaks at 1710 and 1650 cm^{-1} , indicating that the hydrogel and hydrogel nanocomposites were successfully prepared [39]. In the prepared hydrogel bands, the presence of an addition peak at 1161 cm^{-1} indicates that the monomers have been polymerized. Finally, the spectra of LBG-cl-(AA-co-AAm)/TiO₂ HNCs exhibited a new peak at 500 cm^{-1} owing to the Ti–O vibration. The observed functional groups show that both the LBG-based hydrogel, and LBG/TiO₂-based HNCs were successfully synthesized.

The diffractograms of TiO₂ nanoparticles, LBG, LBG-cl-p(AA-co-AAm) hydrogel, and LBG-cl-p(AA-co-AAm)/TiO₂ HNCs are exhibited in Fig. 1b. The X-ray diffractograms of TiO₂ nanoparticles showed clear peaks at $2\theta = 27.44$ (110), 36.06 (101), 41.22 (111), and 54.30 (211), matching the planes of rutile TiO₂ (JCPDS Card No. 21–1276). Also, the TiO₂ nanoparticles had a distinct peak at $2\theta = 25.80$ (101) that related to the anatase TiO₂ plane (JCPDS Card No. 21–1272). These results indicate that both rutile and anatase phases of TiO₂ nanoparticles [23]. In the XRD patterns of LBG, at $2\theta = 18.70^\circ$, a typical amorphous structure appears with a broad band [40–42]. The diffraction intensity increased after grafting AA and AAm, and the diffraction peak for LBG-cl-p(AA-co-AAm) hydrogel shifted slightly ($2\theta = 20.40^\circ$). The single diffraction peak of AA is responsible for this slight shift, indicating no significant structural deformation [41, 42]. Xu et al. [58] discovered in a distinct investigation that pure AA exhibits a solitary diffraction peak at a 2θ value of 20.10° . The co-polymerization of LBG with AA and AAm formed the XRD peak of LBG-cl-p(AA-co-AAm) to exhibit a broadening effect.

On the other hand, the coexistence of crystalline and amorphous phases was noticed in the structure-effect of TiO₂ nanoparticles on the LBG-cl-p(AA-co-AAm) hydrogel. Incorporation of TiO₂ within LBG hydrogel altered its

structure, as shown in the diffractogram of LBG-cl-p(AA-co-AAm)/TiO₂. This material had a strong LBG-cl-p(AA-co-AAm) wide peak with crystalline TiO₂ peaks, indicating that the structure of LBG-cl-p(AA-co-AAm)/TiO₂ HNCs is semi-crystalline (Fig. 1b).

The thermal stability of the TiO₂ nanoparticles, LBG, LBG-cl-p(AA-co-AAm) hydrogel, and LBG-cl-p(AA-co-AAm)/TiO₂ HNCs was determined by the TGA, and data is illustrated in Fig. 1c. TiO₂ nanoparticles were the most thermally stable in the studied range, with the least weight loss residue. LBG showed two decomposition stages. In the first, its weight loss was approximately 3.10% between 25 and 100 °C, because of the water evaporation from polysaccharide structure. In the second stage, the degradation of several monosaccharide units of the polysaccharide structure resulted in a higher rate of weight decomposition from 200 to 370 °C. 21.60% of the residue remained in LBG at 500 °C. The thermograms of LBG-cl-p(AA-co-AAm) hydrogel, and LBG-cl-p(AA-co-AAm)/TiO₂ HNCs showed nearly identical behavior after three thermal events. In the first stage, minimal weight loss occurred between 25 and 200 °C due to the moisture content, whereas in the second stage, 27.00 and 19.00% of the weight loss from 200 to 350 °C for LBG-cl-p(AA-co-AAm) hydrogel and LBG-cl-p(AA-co-AAm)/TiO₂ HNCs, respectively. The disintegration of the backbone polymer chain is responsible for the third weight loss. The final residue amount in HNCs was higher (25.00%) than that in LBG-cl-p(AA-co-AAm) hydrogel (15.00%), indicating significant enhancement the thermal stability after the addition of TiO₂ nanoparticles.

Morphological Characteristics

Figure 2 depicts the morphology and elemental analysis of TiO₂ nanoparticles, LBG, LBG-cl-p(AA-co-AAm) hydrogel and LBG-cl-p(AA-co-AAm)/TiO₂ HNCs. The SEM micrograph of the LBG image appeared smooth (Fig. 2a). The image (Fig. 2b) also clearly shows that after hydrogel formation, the LBG-cl-p(AA-co-AAm) hydrogel has a rough, fragment-like surface. The rough-porous network structure of LBG-cl-p(AA-co-AAm)/TiO₂ HNCs (Fig. 2c) with abundant spherical nanocrystal TiO₂ ps on the polymer hydrogel networks shows successful TiO₂ nanop incorporation, which is compatible with the XRD data. The SEM image in Fig. 3d demonstrated that the TiO₂ NPs size was in the nanoscale range. The image also revealed that the NPs were spherical in shape and uniformly dispersed, and that the TiO₂ nanoparticles had a homogenous structure with no unusual features on the surface. Variable distributions of O and Ti atoms of TiO₂ were observed on the surface of HNCs in the EDS compositional mapping analysis (Fig. 2e). The Ti mapping (Fig. 2f) shows an element with a non-uniform distribution on the polymer surface, whereas the O mapping (Fig. 2g)

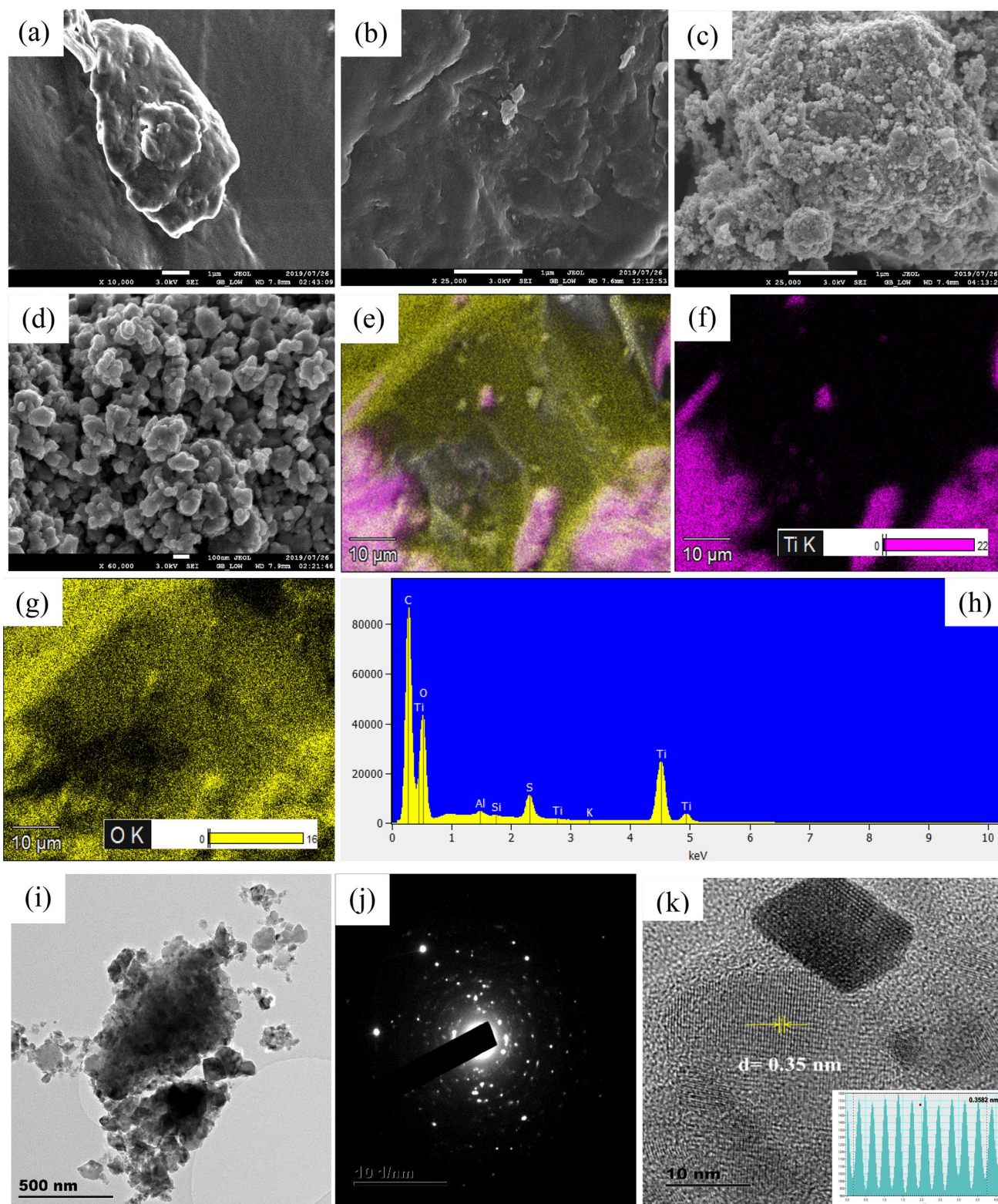


Fig. 2 **a** SEM images of LBG, **b** LBG-cl-p(AA-co-AAm) hydrogel, **c** LBG-cl-p(AA-co-AAm)/TiO₂ HNCs, **d** TiO₂ nanoparticles, **e** EDS of LBG-cl-p(AA-co-AAm)/TiO₂ HNCs, **f** Elemental map of Ti, **g** O

elemental mapping, and **h** EDS analysis of LBG-cl-p(AA-co-AAm)/TiO₂ HNCs, **i** HRTEM images of TiO₂ nanoparticles, **j** SAED pattern of TiO₂ nanoparticles, and **k** HRTEM image of lattice planes

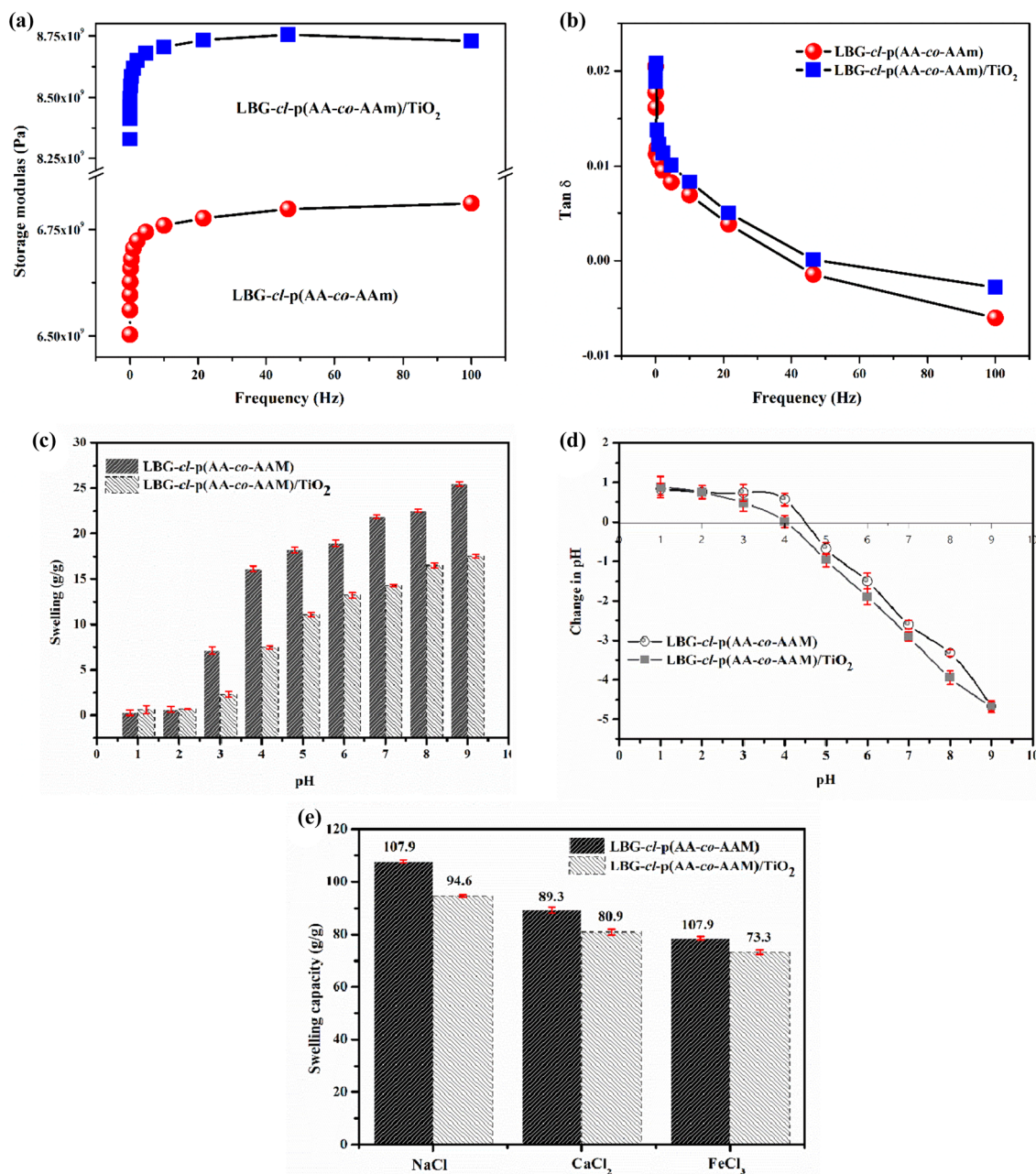


Fig. 3 Frequency dependence of **a** storage modulus, **b** tan of removal by LBG-cl-p(AA-co-AAm) hydrogel and LBG-cl-p(AA-co-AAm)/TiO₂ HNCs. The influence of **c** pH on swelling capacity, **d** pH on sur-

face charge density, and **e** saline on swelling of removal by LBG-cl-p(AA-co-AAm) hydrogel and LBG-cl-p(AA-co-AAm)/TiO₂ HNCs

shows a uniform distribution on the LBG-cl-(AA-co-AAm)/TiO₂ HNCs surface. Addition of TiO₂ nanoparticles in polymer matrix was further elucidated using EDS analysis (Fig. 2h). Furthermore, the EDS-SEM studies confirmed the quantity of titanium (Ti) in the LBG-cl-p(AA-co-AAm)/TiO₂ HNCs, with a weight percentage of 2.79% (Table S1).

HRTEM was used to analyze the morphology of TiO₂ NPs, as shown in Fig. 2. The TiO₂ NPs in Fig. 2i appeared to be spherical, yet they were observed to be

agglomerated. Moreover, TEM images of TiO₂ NPs in various magnifications are shown in Fig. S1. The SAED pattern of the TiO₂ NPs, which consists of several rings, is shown in Fig. 2j. These rings represent the polycrystalline behavior of TiO₂ NPs. The size of the TiO₂ NPs in the TEM image reflects the XRD data. The d-spacing of the TiO₂ nanoparticles configuration was calculated using the fast Fourier transform (FFT) and inverse Fourier transform (IFFT) patterns, as shown in Fig. 2k. The lattice fringes had

an average interlayer spacing of 0.358 nm, which is close to the interlayer spacing of 0.352 nm corresponding to the d-spacing of the (101) planes in anatase TiO₂.

Dynamic Mechanical Analysis

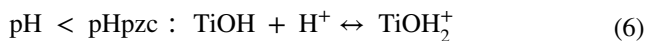
Figure 3a depicts the storage modulus of the synthesized LBG-cl-p(AA-co-AAm) hydrogel and LBG-cl-p(AA-co-AAm)/TiO₂ HNCs as a function of frequency dependence. With increasing frequency, the storage modulus of hydrogel and its HNCs increased. The LBG-cl-p(AA-co-AAm)/TiO₂ HNCs have a higher storage modulus than the corresponding hydrogel based on the storage modulus response to frequency (Fig. 3a). This finding implies that the crosslinking density of the HNCs is greater than that of their hydrogel counterparts due to the higher storage modulus [37]. This might be attributed to better physical interaction in the polymer matrix linkages via links with the inorganic TiO₂ nanofiller [27]. Particularly since TiO₂ nanoparticles are mechanically stable, the homogenous dispersion of TiO₂ nanoparticles in the polymer chains may be responsible for the increased storage modulus [27]. The effect of the hydrogel and its hydrogel nanocomposites on the loss factors ($\tan \delta$) is depicted in Fig. 3b. The $\tan \delta$, which provides details on the properties of the material, is the ratio of viscous energy lost to elastic energy retained. $\tan \delta$ decreases as frequency increases for both LBG-cl-p(AA-co-AAm) hydrogel and LBG-cl-p(AA-co-AAm)/TiO₂ HNCs, indicating that the materials become more elastic.

The swelling behavior of a hydrogel must be determined to examine its usability in a variety of applications. Hydrogels were submerged in solutions ranging from pH 1.0 to 9.0 to investigate their water absorption capacity and reactivity to external pH environments. Figure 3(c) shows that the swelling degrees of LBG-cl-p(AA-co-AAm) hydrogel and LBG-cl-p(AA-co-AAm)/TiO₂ HNCs vary depending on the pHs tested, which are composition-dependent. Despite the fact that both materials exhibited the same swelling behavior across the pH range tested, the hydrogels exhibited a strong swelling tendency. Numerous studies have demonstrated that metal oxide nanoparticles, specifically TiO₂, possess the ability to act as a crosslinking agent with notable crosslinking densities and limited swelling [23, 30]. At high pH, both materials showed significant swelling behavior. The swelling results showed that the LBG-cl-p(AA-co-AAm) hydrogel and LBG-cl-p(AA-co-AAm)/TiO₂ HNCs were pH-dependent. The solution pH in the swelling process is indeed a critical factor affecting the degree of hydrogel ionization. The pH of the solution was modified to induce distinct levels of ionisation in the hydrogel and its nanocomposites present in the initial solution. At low pH ranges, the solution exhibited a depressed swelling on the polymer networks. The elevation

of pH resulted in a concomitant rise in the concentration of -COO- groups, leading to a heightened attraction force. The degree of swelling exhibited a positive correlation with the pH level, resulting in an increase in swelling as pH increased.

The textural characteristics of LBG-cl-p(AA-co-AAm)/TiO₂ HNCs indicate the existence of functional groups on their structure, with carboxyl, hydroxyl, and C-O being the most dominant (Fig. 1a). The pH point of zero charge (pHpzc) of the LBG-cl-p(AA-co-AAm)/TiO₂ HNCs was determined to be 4.4, which closely approximates the pKa of acrylic acid (4.25). The pH point of zero charge (pHpzc) exhibited by the prepared LBG-cl-p(AA-co-AAm)/TiO₂ HNCs indicates a correlation between the pHpzc and the adsorption capacity of the adsorbent employed. It is noteworthy that the present study employed PAA as the primary monomer and AAm as the secondary monomer. It has been established that PAA exhibits ionisation of its carboxylic groups in a pH environment that exceeds its dissociation constant (pKa 4.25) [47]. PAA is an example of an anionic polyelectrolyte that undergoes deprotonation in basic environments. This process results in a significant increase in electrostatic repulsion between the chains, which in turn facilitates water molecule penetration and leads to a substantial swelling of the hydrogel. In an acidic environment, the acidic polymer undergoes protonation, leading to a reduction in charge density and subsequent collapse in polymer volume. On the other side, the introduction of a non-ionic hydrophilic group (-CONH₂) into the LBG-cl-p(AA-co-AAm)/TiO₂ HNCs network results in a low degree of ionisation of -CONH₂ in a nearly neutral environment. The findings indicate that the adsorption of cations is likely to be advantageous when the pH values exceed the pHpzc.

One of the critical elements in determining the mechanism and favorability of the adsorption process is pHpzc. The pHpzc indicator indicates the surface charge on adsorbent surfaces. When the pH of the adsorbents is less than pHpzc, the surfaces gain a net positive charge, which promotes anionic adsorption. When pH exceeds pHpzc, the surface of adsorbents becomes negatively charged, resulting in advantageous cationic adsorption. This is because the adsorbent surface turns negative at higher pH levels (pH > pHpzc), which enhances the electrostatic interactions with cationic MB dye. pHpzc of TiO₂ is usually given as 6.25 to 6.90. In an acidic solution, the surface of TiO₂ nanoparticles appears positively charged (pHpzc > pH) and negatively charged in an alkaline solution (pH > pHpzc), as shown in Eqs. (6) and (7) [51].





The pH_{pzc} of the LBG-cl-p(AA-co-AAm) hydrogel and the pH_{pzc} of the LBG-cl-p(AA-co-AAm)/ TiO_2 HNCs were 4.05 and 4.40, respectively (Fig. 3d). The swelling results showed that LBG-cl-p(AA-co-AAm) hydrogel and the LBG-cl-p(AA-co-AAm)/ TiO_2 HNCs were pH-dependent, which was confirmed by the pH_{pzc} results.

In salt solutions with varying ionic valence values, the swelling behavior of both LBG-cl-p(AA-co-AAm) hydrogel and the pH_{pzc} of the LBG-cl-p(AA-co-AAm)/ TiO_2 HNCs was investigated (Fig. 3e). As the ion concentration increased, the swelling of both adsorbents decreased. Ionic crosslinking points within the polymeric hydrogel network, caused by carboxylate and carboxamide group complexation with multivalent cations, enhance the crosslink density in the hydrogel. The hydrogel matrix contracts as a result, and its ability to expand is reduced. The findings indicate that the swelling degree exhibited a decline as the ionic concentrations (Na^+ , Ca^{2+} , and Fe^{3+}) increased, suggesting that the ionic concentrations had an impact on the swelling degree. It is noteworthy that the extent of swelling in hydrogels decreased significantly as the ionic valence number increased. The deswelling of hydrogel and hydrogel nanocomposites led to a reduction in electrostatic repulsion between $-\text{COO}-$ due to the chelation between $-\text{COO}-$ and metal ions, particularly those with a higher valence number. In addition, the trend revealed a discernible pattern. The order of preference for the adsorbents was observed to be $\text{NaCl} > \text{CaCl}_2 > \text{FeCl}_3$.

Adsorption Studies

In adsorption process, there are different variables were all examined including:

Influence of Solution pH

The pH of adsorption solution is the most essential parameter for adsorbing contaminants from water, as it has the greatest impact on the process. To identify the ideal pH value for this process, the pH influence on removing MB dye was investigated (Fig. S2(a)). As a result, a series of adsorption methods were examined to investigate the MB adsorption efficiency of two adsorbents over a pH range of 4 to 12. When the adsorption solution pH was changed from 4 to 7, the LBG-cl-p(AA-co-AAm) hydrogel and LBG-cl-p(AA-co-AAm)/ TiO_2 HNCs performed better in achieving the MB dye molecules. PAA-based hydrogels are classified as polyelectrolytes owing to the presence of ionizable carboxyl groups within their polymer structure. The PAA-based hydrogels ($\text{pK}_a = 4.25$) exhibit reduced MB dye adsorption under low pH conditions due to the predominant

nonionized state of the COOH groups within the adsorbent structure [47]. Both adsorbents' MB adsorption capacity reached equilibrium at $\text{pH} = 7$. The effectiveness of LBG-cl-p(AA-co-AAm) hydrogel and LBG-cl-p(AA-co-AAm)/ TiO_2 HNCs in an alkaline ($\text{pH} > 7$) environment is demonstrated. The shift in the MB removal curves can be related to adsorption's electrical characteristics and the distribution of MB molecules on the surface. The predominance of carboxyl groups ionizes in an alkaline environment, and according to pH_{pzc} data, the high adsorption efficiency is generated by electrostatic force interactions among MB dye and the adsorbent's surface.

Adsorption behaviour is also affected by the adsorbent dose. The effect of adsorbent dosage was examined (Fig. S2(b)) by adjusting the dosage between 0.5 and 2.5 g/L at pH 7 in 130 mg/L (20 mL) of MB solution for 120 min. The adsorption capability of both adsorbents declined with increasing dosage, and maximal adsorption was attained at a lower (0.5 g/L) polymer concentration. In general, increasing the adsorbent dose reduces adsorption ability because more active sites are inaccessible to the adsorbate. This is because greater doses may promote adsorbent agglomeration and a reduction in active adsorption sites. As shown in the graph of dosage vs. adsorption capacity, the findings for LBG-cl-p(AA-co-AAm) hydrogel and LBG-cl-p(AA-co-AAm)/ TiO_2 HNCs exhibited comparable behavior throughout the examined range.

The experiment on the adsorption kinetics of LBG-cl-p(AA-co-AAm) hydrogel and LBG-cl-p(AA-co-AAm)/ TiO_2 HNCs is shown in Fig. S2(c). Adsorption process consists of two stages such as quick adsorption and gradual equilibrium. The first rapid adsorption stage was because of the distribution of active sites on the adsorbents, which are progressively occupied, and the adsorption equilibrium is established after 80 min. Fig. S2 depicts various kinetic models applied to study the rate of MB adsorption by both adsorbents. The dye concentration effect on the MB removal by both adsorbents was examined at a temperature of 25 °C, as shown in Fig. S2(d). It was found that both adsorbents had a sufficient number of active sites, which, due to an increase in MB concentration, enhanced their adsorption capacity. Moreover, the rise in MB concentration facilitated the transfer and interaction of adsorbate and adsorbents, resulting in increased adsorption capabilities. The data collected for MB adsorption by LBG-cl-p(AA-co-AAm) hydrogel and LBG-cl-p(AA-co-AAm)/ TiO_2 HNCs was modelled and fit using the non-linear isotherm models; plots are illustrated in Fig. S3, while data is displayed in Table 1.

Table 1 The parameters for the MB adsorption kinetic and isotherm models in LBG-cl-p(AA-co-AAm)/TiO₂ hydrogel and LBG-cl-p(AA-co-AAm)/TiO₂ HNCs (above). Non-linear Isotherm parameters for MB dye adsorption onto LBG-cl-p(AA-co-AAm) hydrogel and LBG-cl-p(AA-co-AAm)/TiO₂ HNCs (below)

Linear kinetic models	Kinetic parameters	LBG-cl-p(AA-co-AAm) hydrogel	LBG-cl-p(AA-co-AAm)/TiO ₂ HNCs
Pseudo-first order	K ₁ (/min)	3.7 × 10 ⁻⁵	5.2 × 10 ⁻⁵
	q _e (mg/g)	0.750	1.422
	R ²	0.527	0.626
Pseudo-second order	K ₂ ' (g/mg.min)	0.00098	0.00043
	q _e (mg/g)	398.4	398.4
	R ²	0.999	0.999
Elovich	α (mg/g.min)	2.923	1.332
	β (g/mg)	0.733	0.673
	R ²	0.795	0.824
Intrap diffusion	K _{diff} (mg/g.min ^{0.5})	0.077	0.170
	C	397.2	395.9
	R ²	0.634	0.664
Non-linear isotherm model	Isotherm Constant	LBG-cl-p(AA-co-AAm) hydrogel	LBG-cl-p(AA-co-AAm)/TiO ₂ HNCs
Langmuir	q _m (mg/g)	1540.9	1273.4
	b	0.208	0.180
	R ²	0.986	0.968
	χ ²	2353.1	4717.9
	RMSE	48.51	68.69
Freundlich	K _f (mg/g)	398.3	344.5
	n	2.755	3.221
	R ²	0.867	0.943
	χ ²	9251.4	8390.1
	RMSE	150.0	91.60
Temkin	A _T (L/g)	2.003	2.586
	b _T (J/mol)	7.454	10.42
	R ²	0.973	0.989
	χ ²	4552.6	2575.1
	RMSE	67.47	50.75
Sips	q _m (mg/g)	1406.7	1536.4
	a _s (L/mg)	0.184	0.199
	1/n	1.24	0.704
	R ²	0.993	0.990
	χ ²	1237.9	1541.1
	RMSE	35.18	39.26

Adsorption Kinetic Studies

The performance of MB adsorption in LBG-cl-p(AA-co-AAm) hydrogel and LBG-cl-p(AA-co-AAm)/TiO₂ HNCs was investigated using four adsorption kinetic models: pseudo-first order, pseudo-second order, the Elovich model, and intraparticle diffusion equations. To investigate the adsorption MB mechanism of the adsorption process, the pseudo-first order kinetic [19] and pseudo-second order kinetic [13, 14] models are often used, and their linear equation forms are given in Eqs. (8 and 9):

$$\ln(q_e - q_t) = \ln q_e K_1 - K_1 t \quad (8)$$

$$\frac{t}{q_t} = \frac{1}{k' q_e^2} + \frac{t}{q_e} \quad (9)$$

where q_e (mg/g) is the equilibrium adsorption capacity of adsorbents; K₁ (/min) and K' (g/mg.min) represent pseudo-first order's rate constant and pseudo-second order's rate constant. Equations (8) and (9) were used to linearly fit the experimental observations as shown in Figs. S2 (a) and 6(b). Table 1 shows the calculated isotherm parameters.

The Elovich isotherm model has been widely used to describe chemical adsorption processes in adsorption kinetics models [6]. The linear equation is given in Eq. (10).

$$q_t = \frac{1}{\alpha} \ln(\alpha\beta) + \frac{1}{\alpha} \ln(t) \quad (10)$$

where α is the initial adsorption rate (mg/g.min) and β is a constant proportional to surface coverage (g/mg). Table 1 shows the values of several Elovich constants. In Fig. S2 (c), plots of qt vs $\ln(t)$ with $1/m$ (slope) and the intercepts of C may be used to calculate α and β , respectively.

The intra-particle diffusion model [56] is relevant to molecular diffusion and validates the process of adsorption for MB elimination. Equation (11) depicts the intra-p diffusion model as follows:

$$q_t = K_i t^{1/2} + C \quad (11)$$

where K_i indicates the intra-p diffusion rate constant (mg/g.min^{0.5}) and C denotes the boundary layer influence. The value of C is not zero, as shown in Table 1, showing that diffusion within the ps did not constitute the key rate-determining stage and that the sorption process was fairly complicated because of the boundary layer. During the process, there were two diffusion phases, as illustrated in Fig. S2 (d). The external surface sorption of MB dye molecules from solution was followed by intrap diffusion. The correlation (R^2) values for PSO were higher in the LBG-cl-p(AA-co-AAm) hydrogel and LBG-cl-p(AA-co-AAm)/TiO₂ HNCs than in the other kinetic models studied. According to the findings, the adsorption data agreed with the pseudo-second order model, implying its driven by the adsorption processes.

Adsorption Isotherm

The Langmuir adsorption model is the most widely used form of isotherm in the study of organic dye adsorption. The assumption of uniform adsorption on the adsorbent surface underpins this model. As a result, the Langmuir isotherm is applied to explain the monolayer adsorption process that occurs at identified active sites [20]. The following equation describes the non-linear form of this isotherm (12):

$$q_e = \frac{qmKLCe}{1 + KLCe} \quad (12)$$

where qm (mg/g) is the maximum adsorption capacity, and K_L (L/mg) is the Langmuir constant.

The Freundlich isotherm model is used to describe heterogeneous surfaces. This model is used to describe multisite intermolecular interactions between ions that are adsorbed to active site neighbors, resulting in multilayer adsorption [10]. The Freundlich isotherm model's non-linear form is described by Eq. (13):

$$q_e = KF Ce^{1/n} \quad (13)$$

where K_F is the Freundlich constant for adsorption capacity in (mg/g) and n is the Freundlich constant for adsorption intensity.

The multi-layer chemisorption process is the basis of the Temkin model. The Temkin isotherm model accounts for the adsorbent-adsorbent interaction while ignoring extremely high and low concentration values. The Temkin isotherm is only valid for a narrow range of ion concentrations [53].

The nonlinear Temkin model equation is expressed as follows (14):

$$qe = \frac{RT}{b} \ln(KT_Ce) \quad (14)$$

where K_T is the equilibrium binding constant of the Temkin isotherm (L/g), b is the heat of adsorption constant (J/mol), R is the universal gas constant (8.314 J/mol/K), and T is the equilibrium temperature (273.15 K).

The Sips model is an isotherm hybridizing both the Freundlich and Langmuir models and is widely used to study heterogeneous and homogeneous adsorption systems. This model implies that adsorption only takes place in heterogeneous systems [49]. The equation for the nonlinear Sips isotherm is as follows (15):

$$qe = \frac{q_{ms} a_s C_e^{1/n_s}}{1 + a_s C_e^{1/n_s}} \quad (15)$$

where q_{ms} represents the maximum adsorption capacity (mg/m), a_s represents the Sips constant (L/mg), and n_s represents the Sips isotherm model's exponent, commonly known as the heterogeneity factor. When $1/n_s$ is one, heterogeneous adsorption occurs, but homogeneous adsorption occurs when $1/n_s$ is less than one.

The experimental data from the adsorption processes were fitted to the non-linear isotherm models mentioned above and the results are shown in Fig. S4. The Sips isotherm model describes an appropriate fit to the MB-adsorption for both the LBG-cl-p(AA-co-AAm) hydrogel and LBG-cl-p(AA-co-AAm)/TiO₂ HNCs, as shown by higher R^2 values, low chi-square test statistics (χ^2), and low RMSE values. The exponent $1/n$ value of LBG-cl-p(AA-co-AAm)/TiO₂ HNCs was lower than that of LBG-cl-p(AA-co-AAm) hydrogel. When R^2 , χ^2 , and RMSE for isotherms are analyzed, the MB adsorption data for LBG-cl-p(AA-co-AAm)/TiO₂ HNCs is of the Freundlich type rather than the Langmuir type. The monolayer adsorption capacitance values for LBG-cl-p(AA-co-AAm) hydrogel and LBG-cl-p(AA-co-AAm)/TiO₂ HNCs were 1540.9 and 1273.4 mg/g, respectively, according to the Langmuir model (Table 2). Table 2 compares the maximum adsorption capabilities of the synthesized LBG-cl-p(AA-co-AAm) hydrogel and LBG-cl-p(AA-co-AAm)/TiO₂ HNCs in this work to many other

Table 2 A comparison of the q_{max} of prepared materials with that of existent adsorbents

Hydrogen nanocomposites	Target pollutants	Adsorption kinetics	Adsorption isotherm	q_{max} (mg/g)	References
CMC-cl-PAA/Fe ₃ O ₄ -C30B	MB	PSO	Langmuir	1081.6	[32]
SA-PAA/ZnO	MB	PSO	Langmuir	1529.6	[27]
SA-cl-PAA-TiO ₂	MB	PSO	Langmuir	2257.3	[55]
AgTiO ₂ @AG-g-p (AM-co-AN)	MB	PSO	Langmuir	105.5	[52]
GG-cl-PAAm/TiO ₂ NPs	MB	PSO	Langmuir	1305.4	[33]
GG/poly(AA)/TiO ₂	MG	PSO	Temkim	2145	[23]
GumT-cl-HEMA/TiO ₂	MG	PSO	Langmuir	103.0	[48]
AgTiO ₂ @AG-g-P(AM-co-AN)	MB	PSO	Langmuir	104.5	[52]
Poly(Gg-AAm)ZVI	CR	PSO	Langmuir	153.3	[11]
LBG-cl-(AA-co-AAm) hydrogel	MB	PSO	Sips	1540.9	Present work
LBG-cl-(AA-co-AAm)/TiO ₂	MB	PSO	Sips	1273.4	Present work

poly (Gg-AAm)/ZVI

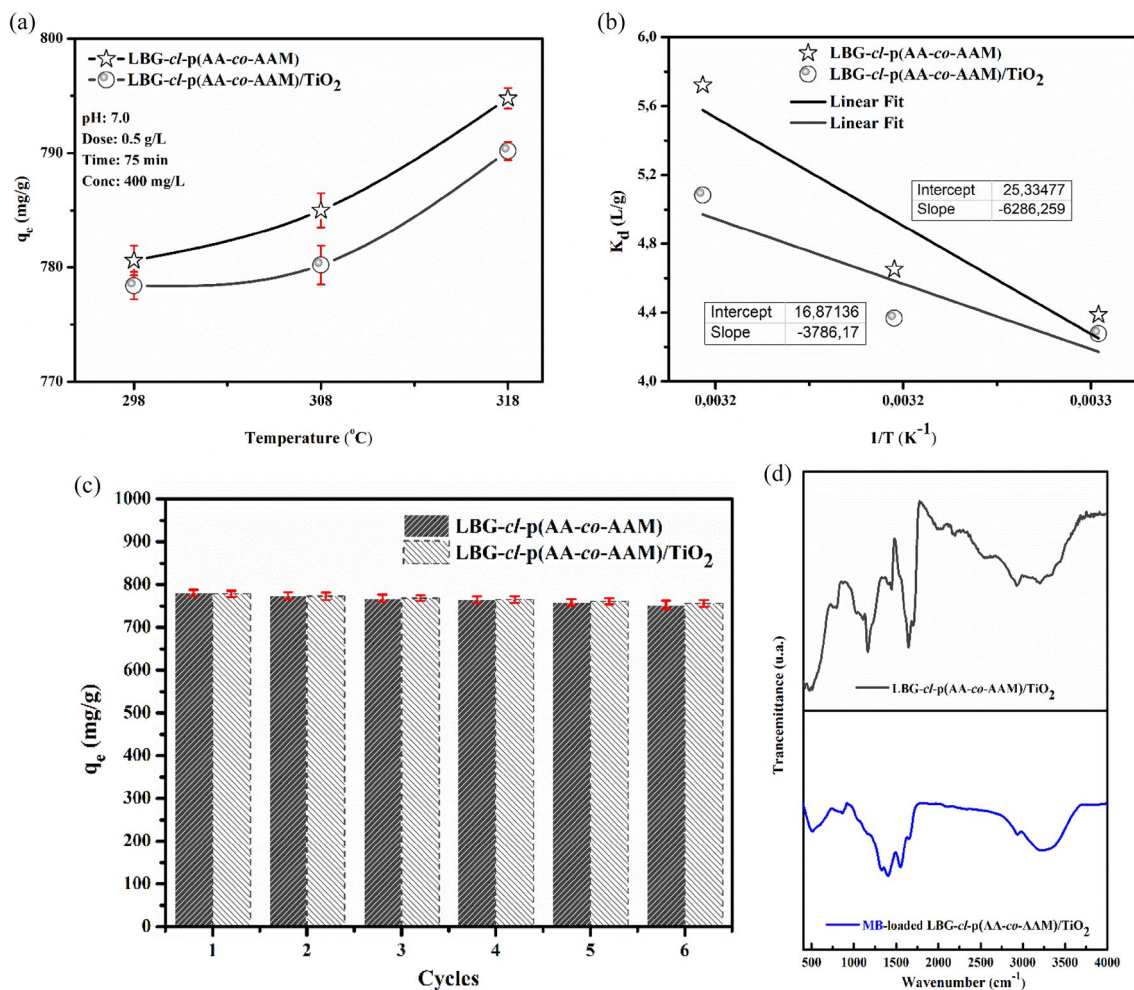


Fig. 4 a The influence of temperature on adsorption c, b the linear Van't Hoff relationship to determine thermodynamic parameters, c regeneration study, and d FTIR of the adsorbents before and after MB adsorption

adsorbent materials described in the literature for MB dye adsorption systems.

Thermodynamics

Figure 4a depicts the temperature influence on MB removal with an adsorbent weight of 0.5 g/L, a pH of 7.0, and 400 mg/L of MB dye. Over a temperature range between 25 and 45 °C, the removal capacities of MB dye on LBG-cl-p(AA-co-AAm) hydrogel and LBG-cl-p(AA-co-AAm)/TiO₂ HNCs increased from 780.6 to 794.8 mg/g and 778.4 to 790.2 mg/g, respectively. It is generally believed that adsorption arises when solvent molecules are displaced at the liquid–solid interface and replaced by MB adsorbate molecules. As a result, an increase in temperature allows additional energy absorption, leading to a weakening of the contact between the liquid surface and the MB molecules. In addition, MB molecule mobility is enhanced, which improves MB adsorption. This is consistent with the observation that the adsorption processes are endothermic.

The temperature effect results were used to calculate the thermodynamic variables of the MB dye adsorption process. Figure 4b shows the linear relationship between $\ln K_d$ and $1/T$ to estimate thermodynamic parameters. The thermodynamic parameters were calculated using Eqs. (15–17) [34]:

$$K_d = m \left(\frac{q_e}{C_e} \right) \quad (16)$$

$$\ln(K_d) = \left(\frac{\Delta S^\circ}{R} \right) - \left(\frac{\Delta H^\circ}{RT} \right) \quad (17)$$

$$\Delta G^\circ = -RT \ln(K_d) \quad (18)$$

where K_d is the equilibrium constant; ΔS° represents the entropy (J/Kmol); ΔH° denotes the enthalpy (kJ/mol); R is the universal gas constant (8.314 J/Kmol); T is the temperature (K) and ΔG° is Gibbs free energy (kJ/mol). Table S2 shows the thermodynamic variables, and the ΔS° value was positive shows a greater degree of randomization of the distribution of adsorbate between the solid and liquid phases. It was clear that the process was endothermic since ΔH° was positive. The negative ΔG° values were verified, showing spontaneous adsorption process over the studied temperature range.

Regeneration

Adsorbent regeneration is one of the most important methods for determining the most efficient adsorbent for wastewater treatment applications. Real-world applications

account for the management of pollutant-loaded adsorbents. It's important to understand that the MB-loaded adsorbent is toxic and difficult to dispose of. As a result, knowing the reusability and recyclability of adsorbent materials is crucial for both the economic and environmental sectors. As the number of adsorption–desorption cycles increased, the adsorption capacity of LBG-cl-(AA-co-AAm)/TiO₂ HNCs decreased with no discernible difference but decreased with a noticeable difference for the corresponding hydrogel (Fig. 4c). After the sixth consecutive cycle, the adsorption ability of MB dyes decreased from 780.6 to 752.7 mg/g and from 778.4 to 756.0 mg/g for LBG-cl-(AA-co-AAm) hydrogel and LBG-cl-(AA-co-AAm)/TiO₂ HNCs, respectively. The trend in adsorption capacity decreased after each cycle because of the loss of active sites as a result of partial desorption. Given the presence of TiO₂ nanoparticles in the LBG-cl-(AA-co-AAm) hydrogel matrix, the high adsorption ability was maintained even after numerous cycles. Furthermore, the improved mechanical properties of the LBG-cl-(AA-co-AAm)/TiO₂ HNCs may be responsible for this result. Table 2 indicates the compatibility of the prepared MB adsorbents with previously published MB adsorbents [27, 32, 52, 55, 33]. In an aqueous solution, the LBG-cl-(AA-co-AAm)/TiO₂ HNCs have a potential adsorption capacity for MB dye.

The efficacy of a specific eluent in removing the adsorbate is contingent upon the interaction between the adsorbate and adsorbent, specifically, the impact of the eluent on the bond formation. The nature of the adsorption mechanism can be determined based on the desorption behaviour of the dye from the adsorbent. If neutral pH water is sufficient to achieve desorption, it suggests weak attachment of the dye to the adsorbent. Conversely, if desorption is facilitated by the use of sulphuric acid or alkaline water, it indicates that the adsorption is likely due to ion exchange. If an organic acid, such as acetic acid, is required to achieve desorption of the dye from the adsorbent surface, it suggests that the dye is chemisorbed onto the adsorbent. Finally, the effect of various reagents used in desorption studies demonstrates that hydrochloric acid is a superior desorption reagent because it can remove over 90% of the adsorbed dye [12]. The choice of eluent for the regeneration process of the MB-loaded adsorbents was determined to be 0.1 M HCl, as per the desorption studies from our previous studies and the literature [24, 28]. In accordance with the adsorption mechanisms, antithetical mechanisms were employed for the purpose of desorbing the adsorbed MB dye from the adsorbents. A plausible desorption mechanism, namely electrostatic exclusion, was postulated. The pH value of a solution containing desorbed MB dye in HCl (0.1 M) was altered, resulting in a modification of the surface charge properties of the MB-loaded samples. At $\text{pH} < \text{pH}_{\text{pzc}}$, the positively charged adsorbents and MB⁺ dye molecules

experience electrostatic repulsion, leading to the effective desorption of adsorbents from MB (Scheme S1).

Insights into the Mechanisms

The elucidation of the chemical structure of the adsorbent before and after MB adsorption may be used to suggest a plausible mechanism of MB adsorption by LBG-cl-(AA-co-AAm)/TiO₂ HNCs (Fig. 4d). It is important to understand that both adsorbent's surface and dye structure have an effect on the adsorption. After MB adsorption, the FTIR spectra of the hydrogel nanocomposites showed a significant change in the peak's position as well as the absorption peak intensities. Notably the removal of existing peaks and development of new peaks were analyzed to determine the nature of the adsorption. After MB adsorption, the broad band's intensity at 2328 to 3694 cm⁻¹ was reduced in LBG-cl-(AA-co-AAm)/TiO₂ HNCs. There is a possibility of intermolecular hydrogen bonding between the surface of the hydrogel nanocomposites and the electronegative nitrogen atoms in the MB molecular structure. Moreover, the peaks at 1648 and 505 cm⁻¹ in the hydrogel nanocomposites had lower absorption intensities after MB adsorption. The disappearance of the monomer-derived peaks at 1155 and 1710 cm⁻¹ shows the electrostatic attraction of MB dye molecules with hydrogel nanocomposites surfaces. The C–H stretching of CH₃ was associated with the appearance of strong peaks at 1550 to 1300 cm⁻¹ in the FTIR of the MB-loaded LBG-cl-(AA-co-AAm)/TiO₂ HNCs. According to the results, electrostatic interactions between the cationic dye (MB) and the negatively charged LBG-cl-(AA-co-AAm)/TiO₂ HNCs surface are crucial to the adsorption process. The point-zero charge and the effect of the solution's pH confirmed the results. Similar results with MB dye adsorption systems have been published in the literature [55, 52, 33]. Accordingly, the interaction mechanism here consists mainly of electrostatic force and hydrogen bonding interactions. A possible adsorption mechanism between MB dye molecules and the hydrogel nanocomposites is shown in Scheme S1.

Conclusion

The study focused on the preparation of LBG-cl-p(AA-co-AAm)-based hydrogel and LBG-cl-p(AA-co-AAm)/TiO₂ HNCs as potential adsorbents for the removal of MB dye from aqueous solution. The developed adsorbents underwent testing using FTIR, XRD, TGA, SEM, TEM, DMA, and point-zero charge methods. The swelling capacity of both adsorbents was examined in various pH solutions. The research findings indicate that the inclusion of TiO₂ NPs had a notable effect on the thermomechanical properties of

the polymeric hydrogel nanocomposites. In addition, it was noted that the inclusion of TiO₂ NPs resulted in a decrease in the hydrogel nanocomposites' ability to swell in water and absorb MB dye. On the basis of the adsorption process, it was observed that both adsorbents were a good match for the Sips isotherm model. Higher confidence values, lower chi-square test statistics, and low RMSE values are in support of this. The Langmuir maximum adsorption capacities of LBG-cl-p(AA-co-AAm) hydrogel and LBG-cl-p(AA-co-AAm)/TiO₂ HNCs were found to be 1540.9 and 1273.4 mg/g, respectively. These values demonstrate their strong potential as effective adsorbents, making them viable alternatives to existing options. A pseudo-second-order model accurately describes the adsorption kinetics results. The thermodynamic parameters of both the hydrogel and HNCs indicate a favourable, predictable, heat-absorbing, and spontaneous adsorption process. After six adsorption/desorption cycles, the adsorbents were able to be regenerated, resulting in a yield of 752.7 mg/g with the hydrogel and 756.0 mg/g with the hydrogel nanocomposites at pH 7. Electrostatic force interactions and weak hydrogen bonding interactions primarily influenced the adsorption process between MB dye molecules and LBG-cl-(AA-co-AAm)/TiO₂ HNCs.

Supplementary Information The online version contains supplementary material available at <https://doi.org/10.1007/s10924-024-03237-1>.

Acknowledgements The authors thank the University of Limpopo for financial support.

Author contribution Boitumelo Rejoice Motshabi: Writing—original draft, Data curation and Formal analysis. Edwin Makhado: Conceptualization, Methodology, Formal analysis, Investigation, Writing—original draft, Data curation, Writing—review and editing. Funding acquisition. Nompumelelo Malatji: Methodology, Investigation, Data curation. Kwena Desmond Modibane: Supervision, Validation, Review and Editing. Mpitloane Joseph Hato: Supervision, Resources, Project administration. Orebotse Joseph Botlhoko: Validation and Methodology. Mahmoud H. Abu Elella: Formal analysis, Writing—review and editing. All authors have read and approved the manuscript version that has been submitted.

Funding Open access funding provided by University of Limpopo.

Declarations

Competing interests The authors declare that they have no financial competing interests.

Open Access This article is licensed under a Creative Commons Attribution 4.0 International License, which permits use, sharing, adaptation, distribution and reproduction in any medium or format, as long as you give appropriate credit to the original author(s) and the source, provide a link to the Creative Commons licence, and indicate if changes were made. The images or other third party material in this article are included in the article's Creative Commons licence, unless indicated otherwise in a credit line to the material. If material is not included in the article's Creative Commons licence and your intended

use is not permitted by statutory regulation or exceeds the permitted use, you will need to obtain permission directly from the copyright holder. To view a copy of this licence, visit <http://creativecommons.org/licenses/by/4.0/>.

References

1. Abu Elella MH, ElHafeez EA, Goda ES, Lee S, Yoon KR (2019) Smart bactericidal filter containing biodegradable polymers for crystal violet dye adsorption. *Cellulose* 26:9179–9206
2. Allouss D, Makhado E, Zahouily M (2022) Recent progress in polysaccharide-based hydrogel beads as adsorbent for water pollution remediation. *Functional polymer nanocomposites for wastewater treatment*. Springer, Heidelberg, pp 55–88
3. Ao C, Zhao J, Li Q, Zhang J, Huang B, Wang Q, Lu C (2020) Biodegradable all-cellulose composite membranes for simultaneous oil/water separation and dye removal from water. *Carbohydr Polym* 250:116872
4. Aswathy SH, Narendrakumar U, Manjubala I (2020) Commercial hydrogels for biomedical applications. *Heliyon* 6(4):e03719
5. Barak S, Mudgil D (2014) Locust bean gum: Processing, properties and food applications—A review. *Int J Biol Macromol* 66:74–80
6. Chien SH, Clayton WR (1980) Application of Elovich equation to the kinetics of phosphate release and sorption in soils. *Soil Sci Soc Am J* 44(2):265–268
7. Darban Z, Shahabuddin S, Gaur R, Ahmad I, Sridewi N (2022) Hydrogel-based adsorbent material for the effective removal of heavy metals from wastewater: a comprehensive review. *Gels* 8(5):263
8. Elella MHA, Aamer N, Mohamed YM, Nazer HAE, Mohamed RR (2023) High-potential removal of copper (II) ions from aqueous solution using antimicrobial crosslinked grafted gelatin hydrogels. *J Polym Environ* 31(3):1071–1089
9. Elella MHA, Goda ES, Gamal H, El-Bahy SM, Nour MA, Yoon KR (2021) Green antimicrobial adsorbent containing grafted xanthan gum/SiO₂ nanocomposites for malachite green dye. *Int J Biol Macromol* 191:385–395
10. Freundlich H (1907) Über die adsorption in lösungen. *Z Phys Chem* 57(1):385–470
11. Goddeti SMR, Bhaumik M, Maity A, Ray SS (2020) Removal of Congo red from aqueous solution by adsorption using gum ghatti and acrylamide graft copolymer coated with zero valent iron. *Int J Biol Macromol* 149:21–30
12. Hema M, Arivoli S (2008) Adsorption kinetics and thermodynamics of malachite green dye onto acid activated low cost carbon. *J Sppl Sci Environ Manag* 12(1):43–46
13. Ho YS, McKay G (1998) Sorption of dye from aqueous solution by peat. *Chem Eng J* 70(2):115–124
14. Ho YS, McKay G (1999) Pseudo-second order model for sorption processes. *Process Biochem* 34(5):451–465
15. Ihaddaden S, Aberkane D, Boukerroui A, Robert D (2022) Removal of methylene blue (basic dye) by coagulation-flocculation with biomaterials (bentonite and *Opuntia ficus indica*). *Journal of Water Process Engineering* 49:102952
16. Inamuddin. (2019) Xanthan gum/titanium dioxide nanocomposite for photocatalytic degradation of methyl orange dye. *Int J Biol Macromol* 121:1046–1053
17. Jack Clifton II, Leikin JB (2003) Methylene blue American journal of therapeutics 10(4):289–291
18. Kaniewska K, Karbarz M, Katz E (2020) Nanocomposite hydrogel films and coatings—Features and applications. *Appl Mater Today* 20:100776
19. Lagergren SK (1898) About the theory of so-called adsorption of soluble substances. *Sven Vetenskapsakad Handlingar* 24:1–39
20. Langmuir I (1918) The adsorption of gases on plane surfaces of glass, mica and platinum. *J Am Chem Soc* 40(9):1361–1403
21. Leng Q, Xu S, Wu X, Wang S, Jin D, Wang P, Dong F (2022) Electrochemical removal of synthetic methyl orange dyeing wastewater by reverse electro dialysis reactor: Experiment and mineralizing model. *Environ Res* 214:114064
22. Makhado E, Hato MJ (2021) Preparation and characterization of sodium alginate-based oxidized multi-walled carbon nanotubes hydrogel nanocomposite and its adsorption behaviour for methylene blue dye. *Front Chem* 9:576913
23. Makhado E, Motshabi BR, Allouss D, Ramohlola KE, Modibane KD, Hato MJ, Pandey S (2022) Development of a ghatti gum/poly (acrylic acid)/TiO₂ hydrogel nanocomposite for malachite green adsorption from aqueous media: Statistical optimization using response surface methodology. *Chemosphere* 306:135524
24. Makhado E, Pandey S, Ramontja J (2018) Microwave assisted synthesis of xanthan gum-cl-poly (acrylic acid) based-reduced graphene oxide hydrogel composite for adsorption of methylene blue and methyl violet from aqueous solution. *Int J Biol Macromol* 119:255–269
25. Makhado E, Pandey S, Ramontja J (2019) Microwave-assisted green synthesis of xanthan gum grafted diethylamino ethyl methacrylate: an efficient adsorption of hexavalent chromium. *Carbohydr Polym* 222:114989
26. Makhado, E., Pandey, S., Kang, M., & Fosso-Kanke, E. (2019, November). Microwave assisted synthesis of xanthan gum-cl-Dimethyl acrylamide hydrogel based silica hydrogel as adsorbent for cadmium (II) removal. In *Int'l Conference on Science, Eng. Technol. and Waste Manag.* 1: 1–6
27. Makhado E, Pandey S, Modibane KD, Kang M, Hato MJ (2020) Sequestration of methylene blue dye using sodium alginate poly (acrylic acid)@ ZnO hydrogel nanocomposite: kinetic, isotherm, and thermodynamic investigations. *Int J Biol Macromol* 162:60–73
28. Makhado E, Pandey S, Nomngongo PN, Ramontja J (2018) Preparation and characterization of xanthan gum-cl-poly (acrylic acid)/o-MWCNTs hydrogel nanocomposite as highly effective re-usable adsorbent for removal of methylene blue from aqueous solutions. *J Colloid Interface Sci* 513:700–714
29. Makhado E, Pandey S, Nomngongo PN, Ramontja J (2019) New horizons in wastewaters management: emerging monitoring and remediation. In: Hauppauge NY (ed) *hydrogel nanocomposites: innovations in nanotechnology for water treatment*. Nova Science Publishers, pp 87–113
30. Malatji N, Makhado E, Modibane KD, Pandey S, Hato MJ (2022) Functional polymer nanocomposites for wastewater treatment, sequestration of organic dyes from wastewater using hydrogel nanocomposites. Springer, Heidelberg, pp 201–223
31. Malatji N, Makhado E, Modibane KD, Ramohlola KE, Maponya TC, Monama GR, Hato MJ (2021) Removal of methylene blue from wastewater using hydrogel nanocomposites: A review. *Nanomaterials and Nanotechnology* 11:18479804211039424
32. Malatji N, Makhado E, Ramohlola KE, Modibane KD, Maponya TC, Monama GR, Hato MJ (2020) Synthesis and characterization of magnetic clay-based carboxymethyl cellulose-acrylic acid hydrogel nanocomposite for methylene blue dye removal from aqueous solution. *Environ Sci Pollut Res* 27:44089–44105
33. Mittal H, Ray SS (2016) A study on the adsorption of methylene blue onto gum ghatti/TiO₂ nanoparticles-based hydrogel nanocomposite. *Int J Biol Macromol* 88:66–80

34. Mittal H, Maity A, Ray SS (2015) Synthesis of co-polymer-grafted gum karaya and silica hybrid organic–inorganic hydrogel nanocomposite for the highly effective removal of methylene blue. *Chem Eng J* 279:166–179
35. Mohamed RR, Abu Elella MH, Sabaa MW, Saad GR (2018) Synthesis of an efficient adsorbent hydrogel based on biodegradable polymers for removing crystal violet dye from aqueous solution. *Cellulose* 25:6513–6529
36. Mohamed RR, Elella MHA, Sabaa MW (2015) Synthesis, characterization and applications of N-quaternized chitosan/poly (vinyl alcohol) hydrogels. *Int J Biol Macromol* 80:149–161
37. Motshabi BR, Ramohlola KE, Modibane KD, Kumar D, Hato MJ, Makhado E (2022) Ultrasonic-assisted synthesis of xanthan gum/ZnO hydrogel nanocomposite for the removal of methylene blue from aqueous solution. *Mater Lett* 315:131924
38. Naserzade SM, Shahrousvand M, Mohammadi-Rovshandeh J, Basati H (2023) Preparation and optimization of photocatalytic polyacrylic Acid/Guar Gum/TiO₂ hydrogels for absorption and removing of methylene blue under visible and UV irradiation. *J Polym Environ* 31(5):2014–2031
39. Nesrinne S, Djamel A (2017) Synthesis, characterization and rheological behavior of pH sensitive poly (acrylamide-co-acrylic acid) hydrogels. *Arab J Chem* 10(4):539–547
40. Pandey S, Do JY, Kim J, Kang M (2020) Fast and highly efficient removal of dye from aqueous solution using natural locust bean gum based hydrogels as adsorbent. *Int J Biol Macromol* 143:60–75
41. Pandey S, Makhado E, Kim S, Kang M (2022) Recent developments of polysaccharide based superabsorbent nanocomposite for organic dye contamination removal from wastewater—A review. *Environ. Res.* 217:114909
42. Pandey S, Son N, Kim S, Balakrishnan D, Kang M (2022) Locust Bean gum-based hydrogels embedded magnetic iron oxide nanoparticles nanocomposite: Advanced materials for environmental and energy applications. *Environ Res* 214:114000
43. Petitjean M, Isasi JR (2022) Locust bean gum, a vegetable hydrocolloid with industrial and biopharmaceutical applications. *Molecules* 27(23):8265
44. Praveen P, Viruthagiri G, Mugundan S, Shanmugam N (2014) Structural, optical and morphological analyses of pristine titanium di-oxide nanoparticles—Synthesized via sol–gel route. *Spectrochim Acta Part A Mol Biomol Spectrosc* 117:622–629
45. Ranjbar-Mohammadi M, Rahimdokht M, Pajootan E (2019) Low cost hydrogels based on gum Tragacanth and TiO₂ nanoparticles: characterization and RBFNN modelling of methylene blue dye removal. *Int J Biol Macromol* 134:967–975
46. Rashid R, Shafiq I, Akhter P, Iqbal MJ, Hussain M (2021) A state-of-the-art review on wastewater treatment techniques: the effectiveness of adsorption method. *Environ Sci Pollut Res* 28:9050–9066
47. Serpe MJ, Jones CD, Lyon LA (2003) Layer-by-layer deposition of thermoresponsive microgel thin films. *Langmuir* 19(21):8759–8764
48. Sharma AK, Kaith BS, Chandel K, Singh A (2020) Bifunctional gelatin/dextrin hybrid backbone based fluorescent chemo-sensor for the detection of tannic acid and removal of eosin yellow dye. *Mater Chem Phys* 254:123304
49. Sips R (1948) On the structure of a catalyst surface. *J Chem Phys* 16(5):490–495
50. Sivakumar R, Lee NY (2022) Adsorptive removal of organic pollutant methylene blue using polysaccharide-based composite hydrogels. *Chemosphere* 286:131890
51. Sun J, Qiao L, Sun S, Wang G (2008) Photocatalytic degradation of Orange G on nitrogen-doped TiO₂ catalysts under visible light and sunlight irradiation. *J Hazard Mater* 155(1–2):312–319
52. Taha GM, Mansor ES, Sultan M (2021) Development of Arabic gum-based AgTiO₂ nanocomposite hydrogel as high efficient adsorbent of cationic dye methylene blue from water. *Int J Biol Macromol* 193:1859–1870
53. Temkin MI (1941) Adsorption Equilibrium and the Kinetics of Processes on Nonhomogeneous Surfaces and in the Interaction between Adsorbed Molecules. *Zhurnal Fiziche- skoi Khimii* 15:296–332
54. Thakur A, Kumar A, Singh A (2024) Adsorptive removal of heavy metals, dyes, and pharmaceuticals: Carbon-based nanomaterials in focus. *Carbon* 217:118621
55. Thakur S, Pandey S, Arotiba OA (2016) Development of a sodium alginate-based organic/inorganic superabsorbent composite hydrogel for adsorption of methylene blue. *Carbohydr Polym* 153:34–46
56. Weber WJ Jr, Morris JC (1963) Kinetics of adsorption on carbon from solution. *J Sanit Eng Div* 89(2):31–59
57. Weerasundara L, Gabriele B, Figoli A, Ok YS, Bundschuh J (2021) Hydrogels: Novel materials for contaminant removal in water—A review. *Crit Rev Environ Sci Technol* 51(17):1970–2014
58. Xu R, Jia M, Zhang Y, Li F (2012) Sorption of malachite green on vinyl-modified mesoporous poly (acrylic acid)/SiO₂ composite nanofiber membranes. *Microporous Mesoporous Mater* 149(1):111–118
59. Zhang W, Tian Y, He H, Xu L, Li W, Zhao D (2020) Recent advances in the synthesis of hierarchically mesoporous TiO₂ materials for energy and environmental applications. *Natl Sci Rev* 7(11):1702–1725
60. Zhou J, Hao B, Wang L, Ma J, Cheng W (2017) Preparation and characterization of nano-TiO₂/chitosan/poly (N-isopropylacrylamide) composite hydrogel and its application for removal of ionic dyes. *Sep Purif Technol* 176:193–199

Publisher's Note Springer Nature remains neutral with regard to jurisdictional claims in published maps and institutional affiliations.